Lateral migration of a ferrofluid droplet in a plane Poiseuille flow under uniform magnetic fields

Md Rifat Hassan and Cheng Wang*

Department of Mechanical and Aerospace Engineering, Missouri University of Science and Technology, Rolla, Missouri 65409, USA

(Received 8 April 2020; accepted 28 July 2020; published 31 August 2020)

The lateral migration of a two-dimensional (2D) viscous ferrofluid droplet in a plane Poiseuille flow under a uniform magnetic field is studied numerically by using the level set method. Focusing on low droplet Reynolds number flows ($\mathrm{Re}_d \leqslant 0.05$), several numerical simulations are carried out to analyze the effects of magnetic field direction and strength, droplet size, and viscosity ratio on the lateral migration behavior of the droplet. The results indicate that the magnetic field direction plays a pivotal role in the trajectory of lateral migration of the droplet and the final equilibrium position in the channel. When the magnetic field is parallel to the channel, i.e., $\alpha = 0^\circ$ (the direction of magnetic field), the droplet is found to settle closer to the wall with an increase in magnetic Bond number Bo_m, while at $\alpha = 45^\circ$, the droplet settles closer to the channel center. Varying the initial droplet sizes at a fixed magnetic Bond number Bo_m and viscosity ratio λ results in different final equilibrium positions within the channel. Additionally, the effect of different viscosity ratios on the migration behavior of the droplet is examined at variable magnetic Bond numbers Bo_m. At $\alpha = 45^\circ$, a critical steady state of deformation is found for $\lambda = 0.5$ and 1 where the droplet changes its migration direction and shifts toward the center of the channel, while at $\lambda = 0.05$, the droplet crosses the center. At $\alpha = 90^\circ$, the droplet is found to settle exactly at the center of the flow domain irrespective of different magnetic Bond numbers, droplet sizes, and viscosity ratios.

DOI: 10.1103/PhysRevE.102.022611

I. INTRODUCTION

Dispersion of droplets in another immiscible fluid is important in a number of industrial applications that deal with natural and synthetic products, including food products, drugs, and milk [1,2]. Dispersion is also important in a variety of technological processes that involve liquid-liquid extraction [3,4] where phase separation is crucial to the purification of the product, such as separation of water from crude oil and separation of glycerol from biodiesel [5].

Crude oil from an oil well contains a significant amount of dispersed water droplets with an average diameter around 50 μm. The volume fraction of water in crude oil must be reduced to less than 0.3% before further processing in order to avoid process equipment corrosion and possibly catalyst poisoning [6,7]. Therefore, understanding the dynamics of droplets in a channel flow, i.e., Poiseuille flow, is of paramount importance to the separation of droplets in the microscale. A single droplet in a pressure-driven flow serves as an excellent model problem to investigate the lateral migration behavior of droplets and can provide fundamental insights on the behavior of more complex phenomena that involves suspension of multiple droplets, e.g., blood flow through blood vessels, tissue and bone passages, and transport of emulsions through porous media [8,9]. In the existing literature, numerous theoretical [10–12], experimental [13,14], and numerical [15,16] studies have been carried out to investigate the migration behavior of droplets in shear flows.

Theoretical investigations on deformed droplets are mostly restricted to the Stokes flow limit. Reversibility of the Stokes flow requires that droplets must be deformed in order to migrate, and small deviations from the spherical shape are considered in all migration theories corresponding to small capillary numbers and small Reynolds numbers. Chan and Leal [17] studied the migration of a nearly spherical drop (small in size compared to the channel width) and obtained a closed form solution for the cross-stream migration velocity in a linear shear flow and two-dimensional Poiseuille flow. They also found that the axial velocity of the drop always lags behind the undisturbed velocity of the flow field. Pak *et al.* [18] and Hanna and Vlahovska [19] analytically attributed the cross-stream migration of a spherical drop toward the center of the channel in a Poiseuille flow due to the effect of surfactant at the drop surface. Zhou and Pozrikidis [20–22] numerically investigated the migration of a deformable drop in a two-dimensional Couette flow and Poiseuille flow at zero Reynolds number and found that the droplet migrates away from the walls. Cross-stream migration of a deformable drop in a two-dimensional Hagen-Poiseuille flow has been studied numerically by Mortazavi and Tryggvason [23], while Afkhami *et al.* [24] performed a two-dimensional numerical analysis to investigate the motion of drops in an unbounded parabolic field. Also, a three-dimensional single droplet migration simulation near a wall in a simple shear flow has been done by Kennedy *et al.* [25].

In order to provide insights into the droplet dynamics in a creeping flow condition, several authors, in their experiments, considered the behavior of solitary drops in linear and parabolic flows. Experimental investigation on the migration of neutrally buoyant drops and solid particles in a tube flow

*wancheng@mst.edu

with a near zero Reynolds number has been performed by Goldsmith and Mason [10,26]. Hiller and Kowalewski [27] conducted experiments on a very dilute suspension of droplets in a plane Poiseuille flow in the limit of creeping flow. These investigations found that at a low viscosity ratio (ratio between the droplet phase viscosity to the continuous phase viscosity), the droplet reached an equilibrium position at the channel axis, whereas at high viscosity ratios the droplet concentration peak moved to a position between the center and the wall of the channel. For a comprehensive review on droplet migration in a Poiseuille flow, readers are referred to Ref. [28], which is an excellent review article.

Due to the very small size of the droplet, settling of droplets by means of only gravitation takes a considerable amount of time. In addition to using viscous shear forces, phase separation can be enhanced by applying external force fields, such as electric or magnetic fields [29,30], which provide an additional means of controlling the dynamics of droplets [31]. Vlahovska [32] performed a perturbation analysis in order to study the effects of drop deformation and shear rheology under a uniform electric field in a shear flow field. Cross-stream migration of a droplet under the effect of a uniform electric field in a Poiseuille flow is analytically investigated by Mandal *et al.* [33], while Feng [34] studied the effect of surface charge convection on the deformation of a drop in a leaky dielectric model at finite Reynolds numbers.

Magnetic fields can also be used to manipulate the shape of a ferrofluid droplet [35,36] or an emulsion system [37]. In particular, the ease of both integration and flexibility of operation render a magnetic field as a popular means of droplet manipulation in microfluidic devices. In order to use magnetic manipulation, either the droplet or the suspending medium needs to be a ferrofluid—a dispersion of magnetic nanoparticles (diameter typically around 10 nm and volume fraction about 5%). Due to the presence of different magnetic properties, Maxwell stresses occur at the fluid-fluid interface in addition to the hydrodynamic stresses. Additionally, multiphase ferrofluid droplets have notable biomedical applications, such as treatment of retinal detachment [38], due to their ability to be delivered to a specific site with the help of proper manipulation of a magnetic field. Liu *et al.* [39] studied the ferrofluid droplet formation under a uniform magnetic field. Afkhami *et al.* [40] numerically investigated the deformation of a neutrally buoyant hydrophobic ferrofluid droplet suspended in a viscous fluid under a uniform magnetic field. Shi *et al.* [41] numerically investigated the dynamics of a falling ferrofluid droplet in a nonmagnetic fluid under the influence of a uniform magnetic field. A thorough investigation on the deformation and orientation of a ferrofluid droplet under uniform magnetic fields has been carried out in our recent work [42].

Until now, only a few have studied the lateral migration behavior of a ferrofluid droplet in a Poiseuille flow under the influence of a uniform magnetic field. Recently, Zhang *et al.* [43] experimentally investigated the effects of magnetic field strength, direction, and interfacial tension on the lateral migration mechanism of a ferrofluid droplet and found that the migration speed increases with an increase in magnetic field strength and a decrease in interfacial tension. However, a comprehensive numerical understanding on the effect of other important parameters (i.e., droplet size and viscosity ratio) on the migration behavior of a ferrofluid droplet in a Poiseuille flow under a uniform magnetic field is missing in the existing literature. Therefore, in this paper, we focus on investigating the lateral migration behavior of a ferrofluid droplet in a plane Poiseuille flow under a uniform magnetic field along a few specific directions. Here a two-dimensional (2D) numerical simulation model is chosen in order to study a wide range of parameters, i.e., magnetic Bond number, droplet size, viscosity ratio, and field direction. Prior studies show that 2D numerical models are capable of qualitatively and correctly capturing the deformation of a ferrofluid droplet under a uniform magnetic field with great computational efficiency [29,30,41,42,44,45]. Our numerical model, built with a commercial FEM solver, models the droplet interface by using the level set method and coupling the magnetic and flow fields.

The remainder of this paper is organized as follows: The numerical model is described in Sec. II. In Sec. III, we present the numerical and mathematical methods that are required to solve our computational model. In Sec. IV, we first validate our model in a Poiseuille flow with different viscosity ratios by comparing our results against the existing theories in the literature and then examine the effect of magnetic field direction, magnetic field strength, droplet size, and viscosity ratio on the migration behavior of the droplet. Finally, the major findings are summarized in Sec. V.

II. NUMERICAL MODEL

Figure 1 schematically represents the suspension of a viscous ferrofluid droplet in another viscous medium in a Poiseuille flow under a uniform magnetic field, $\mathbf{H}_0$. Initially, the viscosity of both phases are matched with each other (i.e., $\eta_d = \eta_c$). Here the magnetic susceptibility of the droplet phase is considered as $\chi_d = 0.25$, while it is zero (i.e., $\chi_c = 0$) in the surrounding phase. The interfacial tension between the two phases is considered as $\sigma = 0.0135$ N/m. Note that the values of interfacial tension and magnetic susceptibility are chosen to be typical for actual experiments.

In the current investigation, all the distances are measured from the center of the droplet, and, initially, a circular ferrofluid droplet with a radius of 75 μm is placed 80 μm below

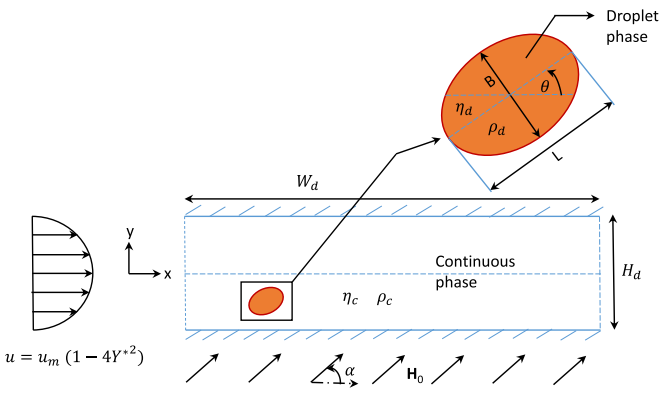

FIG. 1. Schematic representation of a viscous ferrofluid droplet suspended in another viscous medium in a Poiseuille flow under a uniform magnetic field, $\mathbf{H}_0$, at arbitrary directions, α.

TABLE I. Simulation parameters and values.

Parameter	Symbol	Value	Unit
Channel height	H_d	500	μm
Permeability of vacuum	μ_0	$4\pi \times 10^{-7}$	H/m
Initial droplet radius	R_0	75	μm
Interfacial tension	σ	0.0135	N/m
Average flow velocity	u_a	50	mm/s
Density of droplet phase	ρ_d	1000	kg/m^3
Density of continuous phase	ρ_c	840	kg/m^3
Magnetic permeability of droplet phase	μ_d	1.25 μ_0	H/m
Magnetic permeability of continuous phase	μ_c	μ_0	H/m

the center of the domain, which indicates 80-μm vertical separation between the droplet center and center of the flow domain, while it is placed far from the inlet along the horizontal direction to ignore the entrance effect. The velocity at any point in the computational domain can be calculated as $u = u_m(1 - 4Y^{*2})$, where u_m is the maximum flow velocity in the domain, and the velocity profile is symmetric with respect to the x axis along the center of the domain. The dimensionless parameter Y^* defines the relative position of the droplet in the channel along y direction (i.e., $Y^* = \frac{y}{H_d}$). The average velocity at the inlet is taken as 50 mm/s. A no-slip boundary condition is applied to both the top and bottom walls. Additionally, a uniform magnetic field is applied along an arbitrary direction to the flow domain, which is denoted by the angle α. The deformation of the droplet is characterized by the largest dimension L and smallest dimension B along the major and minor axes of the droplet, respectively. The droplet shapes are analyzed in MATLAB to find the properties related to the deformed droplets where the centroid of the droplet is determined by the arithmetic mean of all the points in different coordinate directions. Additionally, when a droplet deforms, it is approximately transformed into an ellipsoidal shape, and the major axis of the droplet refers to the diameter of the ellipsoid along the major-axis direction. Afterward, the orientation angle of the droplet θ is defined as the angle between the major axis of the droplet and positive x axis, measured in the counterclockwise direction. Additionally, for the convenience of the readers, the magnitudes of different parameters that are implemented in the simulations are listed in Table I.

III. NUMERICAL SIMULATION METHOD

A. Level set method

In order to track the dynamic evolution of the droplet interface between the two phases, a conservative level set method is used in our model. The level set method uses an auxiliary scalar step function, ϕ, which has a value of 1 in droplet phase and zero in continuous phase. It varies smoothly from 0 to 1 between the two phases across the interface of the droplet, and $\phi = 0.5$ defines the interface of the droplet. The level set function is governed by the following equation [46]:

$$\frac{d\phi}{dt} + \mathbf{u}\cdot\nabla\phi = \gamma\nabla\cdot\left[\epsilon\nabla\phi - \phi(1-\phi)\frac{\nabla\phi}{|\nabla\phi|}\right], \quad (1)$$

where γ and ϵ denote the amount of reinitialization and the thickness of the droplet interface, respectively. The terms on the left-hand side of the equation represent the motion of the interface, while the terms on the right-hand side are required for numerical stability. The thickness of the interface ϵ is set equal to the largest mesh size of the domain. The reinitialization parameter γ ensures that the level set function gradient remains concentrated to the droplet interface thickness over time, which again needs to be tuned carefully to obtain accurate results. A lower magnitude of γ results in the entrapment of level set function variation in the bulk of one of the fluids, while a higher magnitude leads to smaller time steps and larger computational times. The maximum magnitude of the velocity in the flow domain is considered as a suitable value of γ in level set method. The level set function can also be used to find the unit normal to the interface $\mathbf{n}$:

$$\mathbf{n} = \frac{\nabla\phi}{|\nabla\phi|}. \quad (2)$$

The level set method treats a multiphase flow as a single-phase flow, but the flow properties across the flow domain vary according to the level set function. The properties of the fluids such as density (ρ), dynamic viscosity (η), magnetic permeability (μ), and magnetic susceptibility (χ) can be related to ϕ through the following equations:

$$\rho = \rho_c + (\rho_d - \rho_c)\phi, \quad \eta = \eta_c + (\eta_d - \eta_c)\phi, \quad (3)$$

$$\mu = \mu_c + (\mu_d - \mu_c)\phi, \quad \chi = \chi_c + (\chi_d - \chi_c)\phi, \quad (4)$$

where the subscripts c and d represent the continuous and droplet phases, respectively.

B. Governing equations

The flow field consisting of an incompressible, immiscible ferrofluid droplet suspended in another incompressible, immiscible medium under the application of a uniform magnetic field is governed via the following continuity and momentum equations:

$$\nabla\cdot\mathbf{u} = 0 \quad (5)$$

and

$$\rho\left(\frac{\partial\mathbf{u}}{\partial t} + \mathbf{u}\cdot\nabla\mathbf{u}\right) = -\nabla p + \nabla\cdot\boldsymbol{\tau} + \mathbf{F}_\sigma + \mathbf{F}_m, \quad (6)$$

where p denotes pressure, $\boldsymbol{\tau} = [\eta(\nabla\mathbf{u} + (\nabla\mathbf{u})^T)]$ denotes viscous stress, and $\mathbf{F}_\sigma$ and $\mathbf{F}_m$ represent the surface tension and magnetic forces per unit volume, respectively. The surface tension force $\mathbf{F}_\sigma$ is defined as

$$\mathbf{F}_\sigma = \nabla\cdot[\sigma\{\mathbf{I} + (-\mathbf{n}\mathbf{n}^T)\}\delta], \quad (7)$$

where σ is the coefficient of surface tension, $\mathbf{I}$ is the second-order identity tensor, δ is the Dirac delta function, and $\mathbf{n}$ is the unit normal to the interface that can be calculated using Equation (2). The Dirac delta function δ is approximated using the level set function as

$$\delta = 6|\phi(1-\phi)||\nabla\phi|. \quad (8)$$

TABLE II. Mesh element sizes for grid independence test.

	Mesh 1	Mesh 2	Mesh 3	Mesh 4	Mesh 5	Mesh 6	Mesh 7
Flow field domain	53 870	65 532	82 076	102 976	132 624	143 734	155 866

The magnetic force can be calculated as [47]

$$\mathbf{F}_m = \nabla \cdot \boldsymbol{\tau}_m = \nabla \cdot \left(\mu \mathbf{H}\mathbf{H} - \frac{\mu}{2} H^2 \mathbf{I} \right) \tag{9}$$

where $\boldsymbol{\tau}_m$ is the magnetic stress tensor for the applied magnetic field and $H^2 = \mathbf{H} \cdot \mathbf{H} = |\mathbf{H}|^2$. To calculate the magnetic stress tensor, the magnetostatics equations, including magnetic induction (**B**), magnetization (**M**), and magnetic field (**H**), are solved. Assuming linear and homogeneous material properties, the magnetostatic Maxwell equation relates **B**, **H**, and **M** via the following relationships [48]:

$$\nabla \cdot \mathbf{B} = 0, \quad \nabla \times \mathbf{H} = 0, \quad \mathbf{M} = \chi \mathbf{H}, \quad \text{and}$$
$$\mathbf{B} = \mu_0(\mathbf{H} + \mathbf{M}) = \mu_0(1 + \chi)\mathbf{H}, \tag{10}$$

where $\mu_0 = 4\pi \times 10^{-7}\,\mathrm{N/A^2}$ is the permeability of vacuum and μ and χ depend on the phase function ϕ according to Eq. (4). A scalar potential ψ can be defined, and its gradient represents curl-free **H** (i.e., $\mathbf{H} = -\nabla\psi$). We can now write

$$\nabla \cdot (\mu \nabla \psi) = 0. \tag{11}$$

C. Governing equations in nondimensional form

Now we rewrite the governing equations into nondimensional forms to understand the effect of different nondimensional groups on the droplet dynamics. The length and time are scaled by the height of the channel H_d and the inverse of the average shear rate $\dot{\gamma}_a$, respectively. The parameter $\dot{\gamma}_a$ can be defined as $\frac{2u_a}{H_d}$, where u_a is the average velocity in the flow domain, which again equals 2/3 times the maximum velocity u_m in the flow domain (i.e., $u_a = \frac{2}{3}u_m$). The other dimensional variables are converted to nondimensional forms through the following relationships:

$$X^* = \frac{x}{H_d}, \quad Y^* = \frac{y}{H_d}, \quad R^* = \frac{R_0}{H_d}, \quad p_a^* = \frac{p}{\eta \dot{\gamma}_a}$$
$$\rho^* = \frac{\rho}{\rho_c}, \quad \eta^* = \frac{\eta}{\eta_c}, \quad \mu^* = \frac{\mu}{\mu_0}, \quad \mathbf{H}^* = \frac{\mathbf{H}}{H_0},$$

where H_d is the channel height and H_0 is the magnitude of the externally applied magnetic field $\mathbf{H}_0$. Therefore, governing equations (5) and (6) can be written as

$$\nabla^* \cdot \mathbf{u}^* = 0 \tag{12}$$

and

$$\mathrm{Re}_d \left(\rho^* \frac{D\mathbf{u}^*}{Dt^*} \right) = -\nabla^* p_a^* + \nabla^* \cdot \tau^* + 2\frac{\mathrm{Bo}_m}{\mathrm{Ca}} \nabla^* \cdot \boldsymbol{\tau}_m^* + \frac{1}{\mathrm{Ca}} \mathbf{F}_\sigma^*. \tag{13}$$

In the above equations, the superscript $*$ represents the nondimensional variables. The different dimensionless groups are the droplet Reynolds number (Re_d), average capillary number (Ca), and magnetic Bond number (Bo_m), which are defined as follows:

$$\mathrm{Re}_d = \frac{\rho_c R_0{}^2 \dot{\gamma}_a}{\eta_c}, \tag{14}$$

$$\mathrm{Ca} = \frac{\eta_c R_0 \dot{\gamma}_a}{\sigma}, \tag{15}$$

and

$$\mathrm{Bo}_m = \frac{R_0 \mu_0 H_0{}^2}{2\sigma}. \tag{16}$$

The viscosity ratio λ and permeability ratio ζ are also defined as follows:

$$\lambda = \frac{\eta_d}{\eta_c} \quad \text{and} \quad \zeta = \frac{\mu_d}{\mu_0}. \tag{17}$$

Here we will mainly concentrate on the effects of Bo_m, α, R_0, and λ on the lateral migration behavior of the droplet in low droplet Reynolds number flows ($\mathrm{Re}_d \lesssim 0.05$).

D. Grid independence test

A grid independence test is performed to determine the optimum size of the mesh elements that gives accurate results, while saving a reasonable amount of computational time. In this case, we have used different mesh sizes and compared the lateral migration behavior of the droplet. Different triangular mesh element sizes for the grid independence test are tabulated in Table II, and Fig. 2 represents the lateral migration of the droplet Y_d^* for the respective configurations. It can be seen that when there are more than 132,624 elements in the flow field domain, the lateral migration profiles of the droplet (Meshes 6 and 7) completely overlap with each other. We have

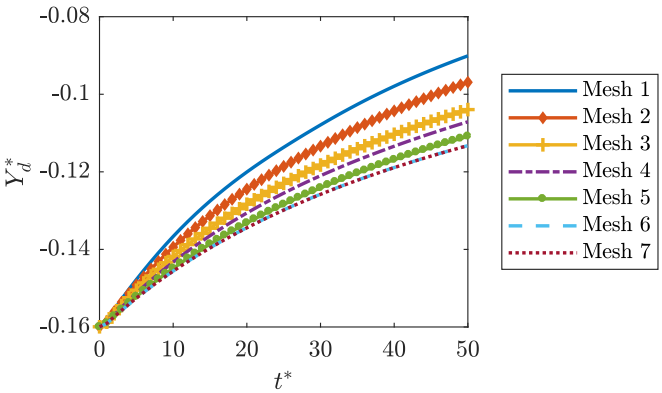

FIG. 2. Grid independence test: The time evolution of lateral migration behavior of the droplet, Y_d^*, for different mesh configurations: Mesh 1, blue (solid) line; Mesh 2, orange (diamond) line; Mesh 3, yellow (plus) line; Mesh 4, violet (dash-dot) line; Mesh 5, green (circle) line; Mesh 6, cyan (dashed) line; and Mesh 7, maroon (dotted) line.

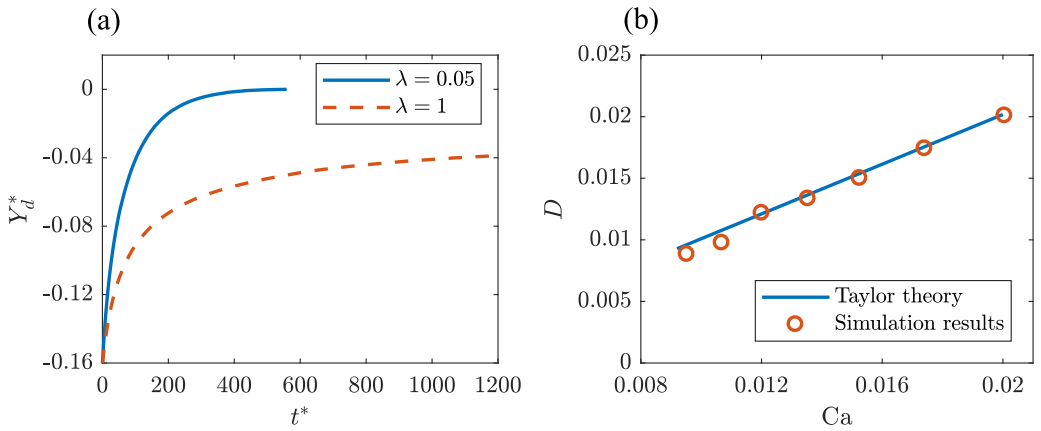

FIG. 3. Time evolution of droplet trajectory in a Poiseuille flow at $\mathrm{Re}_d = 0.03$ and $\mathrm{Bo}_m = 0$. (a) Lateral migration of droplet for different viscosity ratios, Y_d vs. t^*; (b) comparison of simulated droplet deformation D results against Taylor's theory at variable capillary numbers, D vs. Ca at $\lambda = 0.05$.

used 143 734 elements for the simulations throughout the rest of the paper.

IV. RESULTS AND DISCUSSIONS

A. Validation of numerical method

Droplet migration in a Poiseuille flow

At first, we validated our model by comparing the results against the existing theories in the literature in terms of the lateral migration of a droplet in a Poiseuille flow for different viscosity ratios at $\mathrm{Re}_d = 0.03$ and $\mathrm{Bo}_m = 0$. The most thorough theoretical analysis on droplet migration behavior in a two-dimensional Poiseuille flow is given by Chan and Leal [17], who considered the effect of the deformed shape of the droplet as a critical factor on the droplet trajectory motion in a unidirectional shear flow. Two different hydrodynamic interactions are mainly responsible for droplet migration. First is the interaction between the deformed drop and the bottom wall of the channel, which causes the droplet to migrate away from the bottom wall toward the center of the flow domain, and this interaction gradually decreases as the distance between the droplet and bottom wall increases. Second is the interaction between the deformed drop and the flow field, which vanishes in a simple shear flow but plays an important role in the quadratic flow field [27]. According to Chan and Leal [17], the migration behavior of the droplet due to its interaction with the flow field is essentially dependent on the viscosity ratio λ. When $\lambda < 0.5$ and $\lambda > 10$, both types of interactions act in the same direction, and the droplet migrates toward the centerline of the channel. On the other hand, for intermediate values of viscosity ratios ($0.5 < \lambda < 10$), the interaction of the deformed droplet with the velocity profile forces the droplet to migrate toward the bottom wall. Since, for $0.5 < \lambda < 10$, both types of interactions take place at the same time and are in opposite directions, the droplet finds a steady-state position at some point between the center and the bottom wall of the channel due to the combined effect of these forces. Moreover, it is important to note that this equilibrium position where the two forces become equal also depends on the relative size of the droplet [27]. Experimental investigations of Karnis and Mason [10] show that a single drop moves away from the wall in a pressure-driven channel flow and reaches the center of the channel for low viscosity ratios. Furthermore, Hiller and Kowaleski [27] experimentally found the highest drop number density at the center line for the low viscosity ratio (i.e., $\lambda = 0.1$), while for the moderate viscosity ratio (i.e., $\lambda = 1$), the highest concentration was located at a position between the center and the wall.

Figure 3(a) represents the lateral migration behavior of a droplet for different viscosity ratios. It can be seen that when $\lambda = 0.05$, the droplet migrates toward the center of the channel. On the other hand, at $\lambda = 1$, the droplet settles down at a point between the center and wall of the channel. Both simulation results qualitatively agree well with the existing theories in the literature.

We also validated the deformation of the droplet D at different positions in the channel against Taylor's theory. According to Taylor [49,50], the deformation of a neutrally buoyant droplet suspended in another incompressible and immiscible viscous medium at the Stokes flow limit under a simple shear flow can be calculated as

$$D = \frac{L - B}{L + B} = \frac{19\eta_d + 16\eta_c}{16\eta_d + 16\eta_c}\mathrm{Ca}, \tag{18}$$

where the average capillary number Ca is defined in Eq. (15). Equation (18) is based on the assumption of an unbounded shear flow and a vanishing Reynolds number. Figure 3(b) illustrates the comparison of simulation results against Taylor's theory, which are in very good agreement with each other. Additionally, we validated the ferrofluid droplet deformation in a quiescent flow under a uniform magnetic field in our previous work [42].

B. Lateral migration behavior of a droplet under uniform magnetic fields

1. Effect of magnetic field direction

When a magnetic field is applied to a ferrofluid droplet in a Poiseuille flow, the droplet undergoes deformation due to the combined effect of the shear flow and the magnetic field [42]. Here, in this section, we investigate the effect of magnetic field

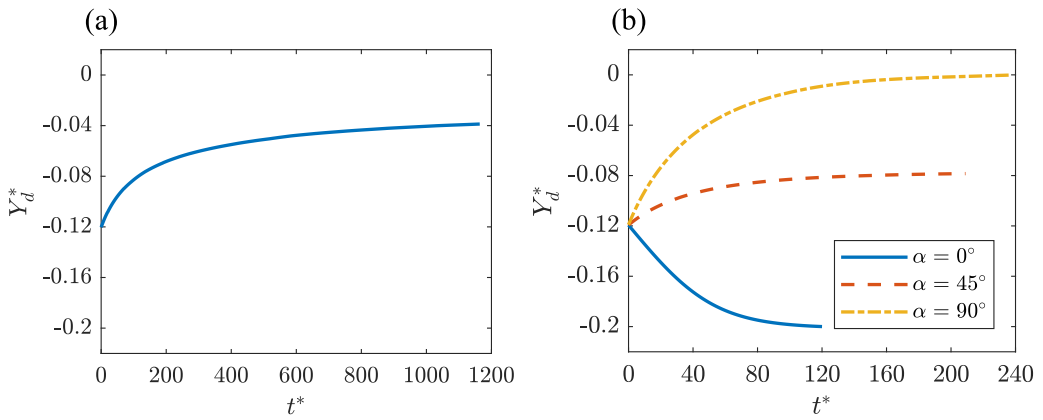

FIG. 4. Effect of different magnetic field directions on the migration behavior of the droplet at $\mathrm{Re}_d = 0.03$ and $\lambda = 1$. (a) $\mathrm{Bo}_m = 0$ and (b) $\mathrm{Bo}_m = 8.72$.

directions on the lateral migration behavior of the ferrofluid droplet suspended in a parabolic flow field. For the subsequent studies, we will use a droplet Reynolds number, $\mathrm{Re}_d = 0.03$ and $\lambda = 1$.

Figure 4 shows the effect of different magnetic field directions on the migration behavior of the droplet. Here we have chosen some representative α for better illustration of the results. From Fig. 4(a), we can see that in the absence of any magnetic field, at $\lambda = 1$, the droplet finally settles down approximately 0.038 below the center of the channel, which also takes a considerable amount of time to reach the equilibrium position. In contrast, from Fig. 4(b), it can be seen that applying a uniform magnetic field from different arbitrary directions results in different final equilibrium positions along the channel relatively in a shorter period of time. Interestingly, we can also see that the droplet follows different trajectories before reaching the final equilibrium position. For example, when $\alpha = 45°$ and $90°$, the droplet migrates upward, while at $\alpha = 0°$, the droplet migrates downward. A magnetic field strength of $H_0 = 50\,000$ A/m is used in all these cases, which corresponds to a magnetic bond number equal to 8.72. Figure 5 depicts the steady-state velocity, magnetic field profiles, and equilibrium droplet shapes at $\mathrm{Re}_d = 0.03$ and $\mathrm{Bo}_m = 8.72$. It can be seen that the droplet undergoes deformation and tends to orient itself along the direction of the magnetic field, which is also consistent with our previous findings [42]. At $\alpha = 90°$, the droplet shape is found to be symmetric with respect to the x axis, which in turn aids the droplet to settle at

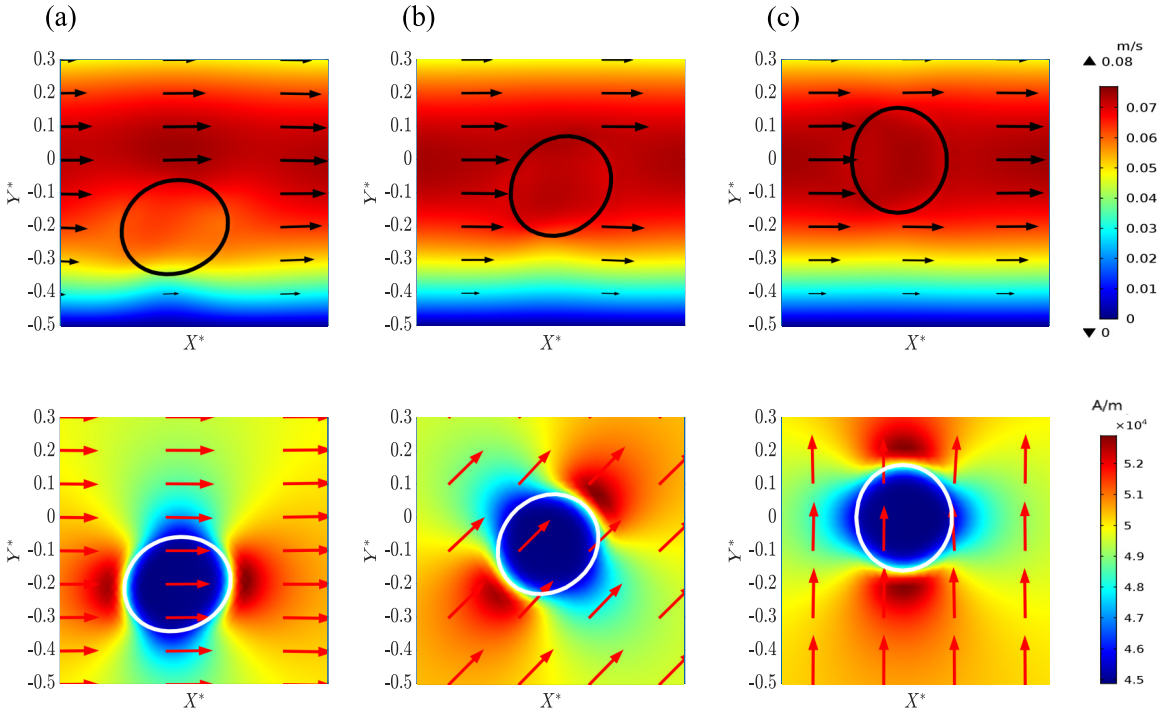

FIG. 5. Steady-state velocity, magnetic field profiles, and equilibrium droplet shapes at $\mathrm{Re}_d = 0.03$ and $\mathrm{Bo}_m = 8.72$. (a) $\alpha = 0°$, (b) $\alpha = 45°$, and (c) $\alpha = 90°$.

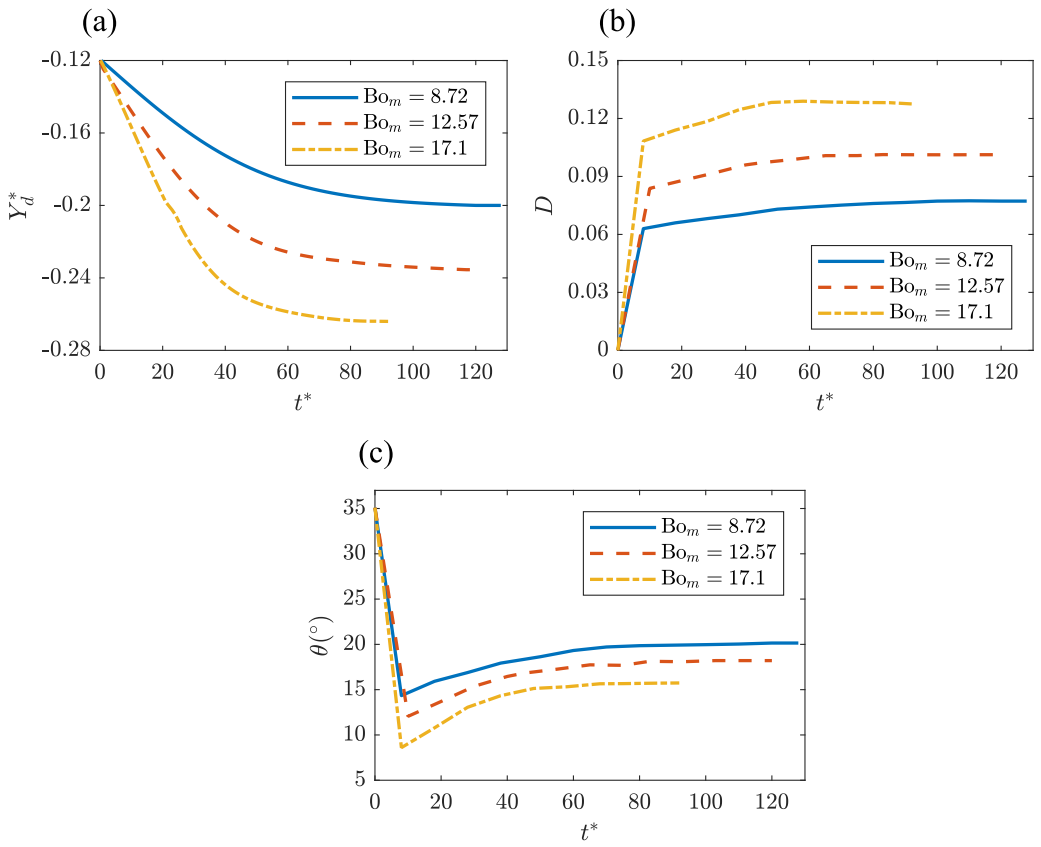

FIG. 6. Effect of magnetic field strengths, H_0, on the migration behavior of the droplet at $\alpha = 0^\circ$, $\mathrm{Re}_d = 0.03$, and $\lambda = 1$. (a) Y_d^* vs. t^*, (b) D vs. t^*, and (c) θ vs. t^*.

the center of the channel. Contrarily, at $\alpha = 0^\circ$ and 45°, due to the asymmetry in the shape of the droplet, the droplet experiences different hydrodynamic interactions along the interface of the droplet, which force it to find an equilibrium position at a point somewhere between the center and the bottom wall of the channel. The flow field becomes more distorted as the droplet tends to further align itself in the vertical direction to conform to the droplet shape. From the magnetic field profiles, it can be seen that the droplet experiences maximum magnetic field strength along the direction the magnetic field is applied, while the strength is least in magnitude in the other orthogonal direction. The magnetic field is also uniform both inside and far outside the droplet. Additionally, the magnetic field lines are parallel to each other; however, they are slightly deflected at the interface of the droplet due to the change in magnetic susceptibility at the interface. Therefore, it is clear that the different droplet shapes and their alignment with the flow field along with hydrodynamic interactions play a crucial role in the trajectory of the lateral migration and the final equilibrium position in a channel.

2. *Effect of magnetic field strength*

External force fields, i.e., magnetic fields, electric fields are capable of inducing topological changes to a droplet suspended in another medium, and in the previous section, we observed that the magnetic field direction can significantly influence the final equilibrium position of a ferrofluid droplet in a channel flow. Now, we apply variable magnetic field strengths along different directions to analyze how they affect the lateral migration behavior of the droplet at $\lambda = 1$.

a. $\alpha = 0^\circ$. Figure 6 illustrates the effect of different magnetic field strengths on the migration behavior of the droplet at $\alpha = 0^\circ$. From Fig. 6(a), it can be seen that as the magnetic field strength increases, the droplet moves closer to the bottom wall of the channel, while the droplet was found to settle closer to the center of the channel in the absence of any external forces. The droplet settles faster at the equilibrium position at a higher magnetic field strength. This is because with increasing magnetic field strength, the droplet undergoes greater deformation, which is clearly demonstrated in Fig. 6(b). Additionally, if we look at the trend in the orientation angle of the droplet in Fig. 6(c), then it can be seen that with increasing magnetic field strength, the orientation angle decreases. This is because as the droplet moves closer to the wall, the shear rate increases, which in turn reduces the orientation angle values of the droplet [42]. Moreover, the increasing magnetic field strength forces the droplet to align itself more toward the direction of the magnetic field. As a result, the resultant between the direction of the flow field and magnetic field decreases, i.e., the orientation angle decreases. In this case, the deformation of the droplet in combination with the orientation angle plays a pivotal role in determining the final equilibrium position of the droplet.

b. $\alpha = 45^\circ$. When we apply the magnetic field at 45°, it can be seen from Fig. 7(a) that the droplet migrates upward toward the center of the channel, and as the magnetic field strength increases, it migrates further away from the bottom

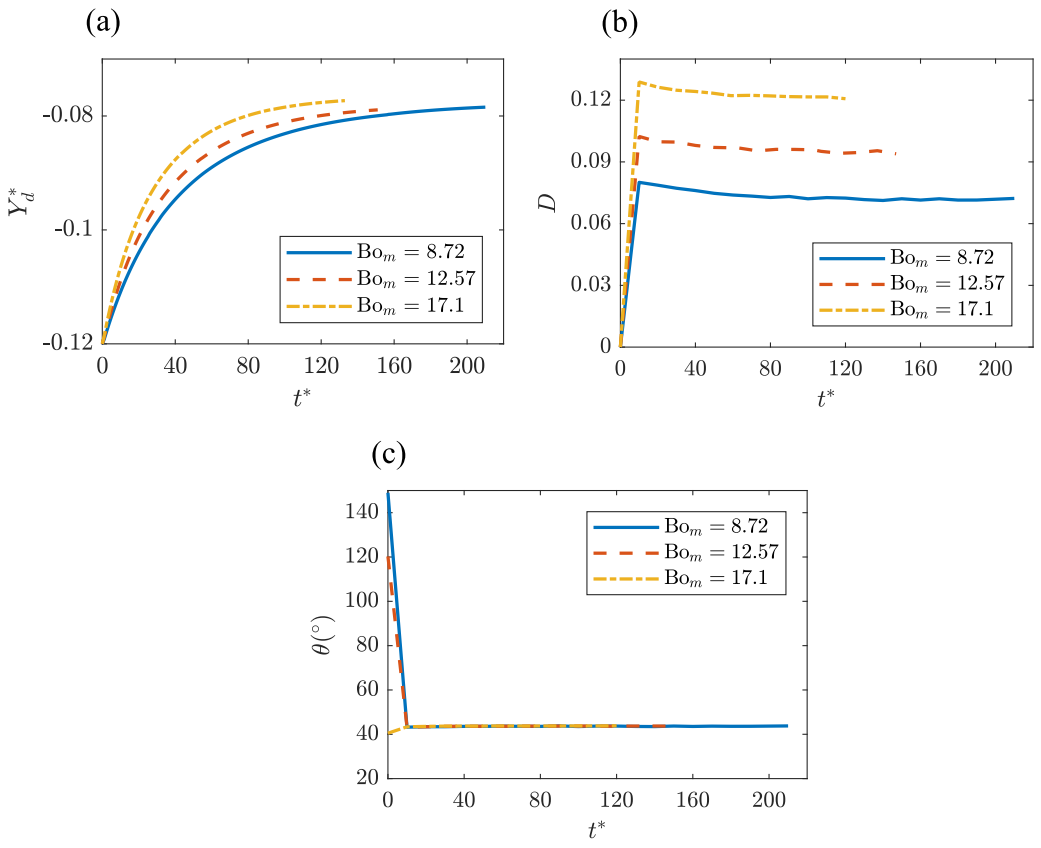

FIG. 7. Effect of magnetic field strengths, H_0, on the migration behavior of the droplet at $\alpha = 45^\circ$, $\mathrm{Re}_d = 0.03$, and $\lambda = 1$. (a) Y_d^* vs. t^*, (b) D vs. t^*, and (c) θ vs. t^*.

wall of the channel; however, the change in migration rate is much smaller in this case compared to each other. The primary reason behind the migration behavior is related to the deformation of the droplet, which increases with increasing magnetic field strength [Fig. 7(b)]. In addition, it takes less time to reach a steady state at a higher magnetic field strength, which is similar to the previous case mentioned above. Figure 7(c) represents the orientation angle for all cases. It can be seen that the results overlap with each other, and the orientation angle reaches a saturation point, which is close to the direction along which the magnetic field is applied. Since the orientation angle remains the same irrespective of different magnetic field strengths, in this case, it is clear that droplet deformation is crucial to the final equilibrium position of the droplet.

c. $\alpha = 90^\circ$. Finally, we applied the magnetic field along a direction perpendicular to the direction of the flow field to observe its effect on the lateral migration behavior of the droplet. We can see from Fig. 8(a) that the droplet finally settles at the center of the channel for all the cases, and with increasing magnetic field strength, the droplet settles faster in the equilibrium position. The reason behind this can be attributed to the droplet deformation trend with increasing magnetic field strength [Fig. 8(b)]. Figure 8(c) represents the orientation angle trends of the droplet, and it is clear that at a steady-state condition, the orientation angle becomes approximately equal to 90° for all the cases. Additionally, the steady-state droplet shape is found to be symmetric with respect to the center of the domain, which also helps the droplet to maintain the final equilibrium position at the center of the channel. Therefore, the results show that at a fixed viscosity ratio, the final equilibrium position of the droplet in a Poiseuille flow can be manipulated by means of applying magnetic fields of different strengths along various directions.

3. Effect of droplet size

In this section, we investigate the dependence of the migration behavior of the droplet on different initial droplet sizes at $\lambda = 1$. Like previous sections, surface tension and magnetic susceptibility of the ferrofluid droplet are kept constant, i.e., $\sigma = 0.0135$ N/m and $\chi_d = 0.25$, while the droplet aspect ratios R_0^* are varied from 0.11 to 0.24. Here we also apply the magnetic field in arbitrary directions to observe its effect on the final equilibrium position of the droplet in the channel.

a. $\alpha = 0^\circ$. Figure 9 illustrates the effect of different droplet sizes on the migration behavior of the droplet at $\alpha = 0^\circ$. From Fig. 9(a), it can be seen that when the magnetic field is applied, the droplet starts to migrate downward, and as the droplet size increases, it settles at a position far away from the bottom wall. This behavior can be directly attributed to the deformed shape of the droplet. Figure 9(b) shows that with the increase in the size of the droplet, the deformation of the droplet increases, and this phenomenon can be explained by the definition of the magnetic Bond number [Eq. (16)]. Since the magnetic Bond number is directly proportional to the size of the droplet, as the droplet size increases, the magnetic force becomes larger compared to the interfacial force, i.e., droplet deformation

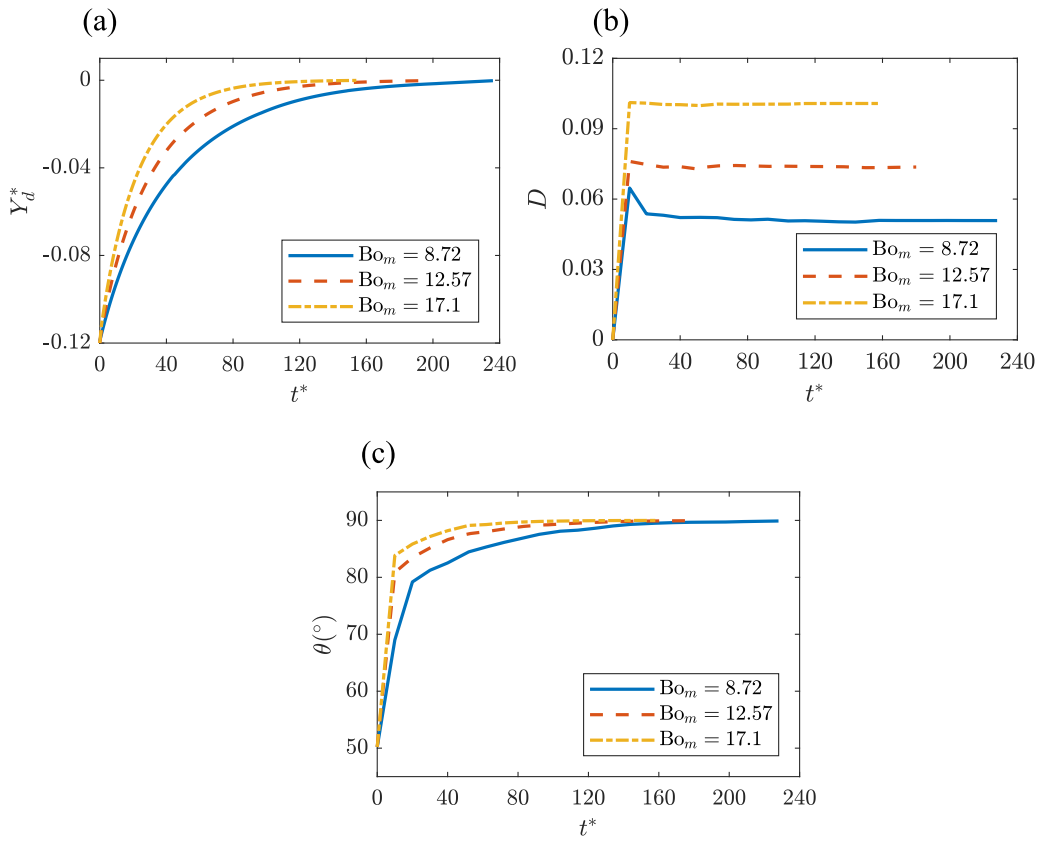

FIG. 8. Effect of magnetic field strengths, H_0, on the migration behavior of the droplet at $\alpha = 90^\circ$, $\mathrm{Re}_d = 0.03$, and $\lambda = 1$. (a) Y_d^* vs. t^*, (b) D vs. t^*, and (c) θ vs. t^*.

increases. Consequently, as the droplet becomes larger, the gap between the deformed droplet and bottom wall decreases, which in turn increases the force exerted by the wall, and therefore the centroid of the droplet is pushed further away from the bottom wall. Furthermore, the droplet reaches its final equilibrium position faster with an increase in the initial size of the droplet.

b. $\alpha = 45^\circ$. Now we apply the magnetic field along $\alpha = 45^\circ$ to analyze its effect on the final equilibrium position of different initial sized droplets. Figure 10 represents the effect of different droplet sizes, R_0^*, on the migration behavior of the droplet at $\alpha = 45^\circ$, and it can be seen from Fig. 10(a) that for all initial sizes, the droplet migrates away from the bottom wall, and with an increase in droplet size, it moves closer to the center of the channel. Additionally, as the droplet size increases, the droplet finds its equilibrium position along the flow domain in a relatively short period of time. Similarly to the previous case mentioned above, this migration behavior is also related to the deformation of the droplet. As we can see from Fig. 10(b), the droplet undergoes a larger deformation

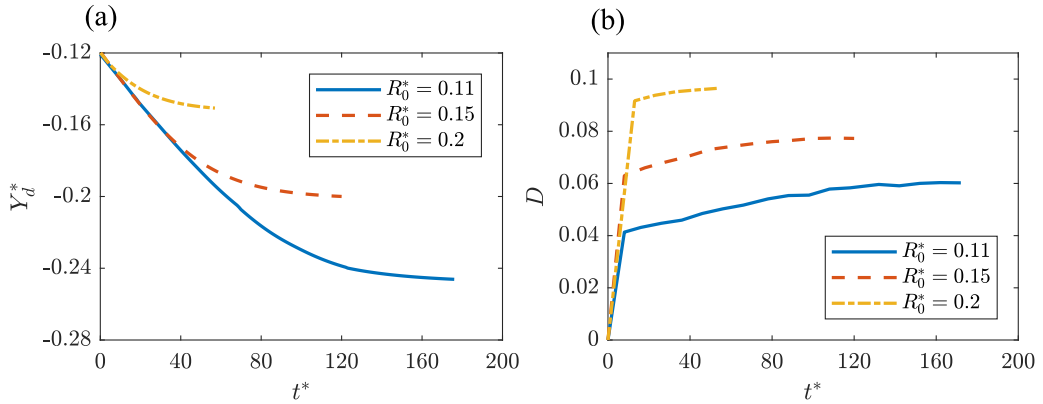

FIG. 9. Effect of different droplet sizes, R_0^*, on the migration behavior of the droplet at $\alpha = 0^\circ$, $\mathrm{Re}_d = 0.03$, and $\lambda = 1$. (a) Y_d^* vs. t^* and (b) D vs. t^*.

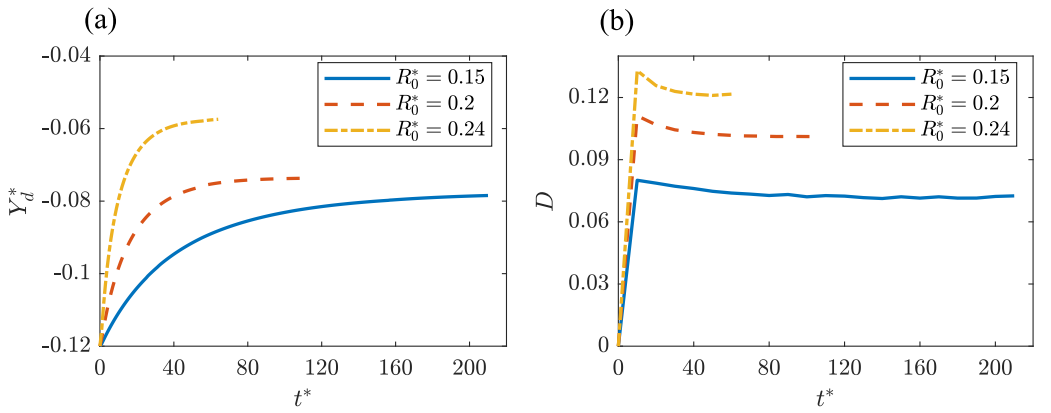

FIG. 10. Effect of droplet sizes, R_0^*, on the migration behavior of the droplet at $\alpha = 45^\circ$, $\mathrm{Re}_d = 0.03$, and $\lambda = 1$. (a) Y_d^* vs. t^* and (b) D vs. t^*.

and reaches a steady-state deformation faster with an increase in the initial droplet sizes. Furthermore, the droplet is found to orient itself along the direction of the magnetic field where the orientation angle reaches a saturation point close to 45°.

c. $\alpha = 90^\circ$. Finally, we apply the magnetic field along a direction perpendicular to the flow domain to observe how this arbitrary direction affects the settling of the droplet for different initial size conditions. In this case, we can see from Fig. 11(a) that the droplet finds its equilibrium position at the center of the channel irrespective of the initial size conditions. With an increase in the droplet size, the deformation of the droplet increases [Fig. 11(b)], which in turn helps the droplet to reach the equilibrium position faster at the center of the flow domain. When the magnetic field is applied, the droplet tries to align itself toward the direction of the magnetic field due to the dominant nature of the magnetic field at a low capillary number, and the orientation angle of the droplet becomes approximately 90° for all the cases. Additionally, this symmetric shape of the droplet aids the droplet in maintaining its equilibrium position at the center.

Figure 12 illustrates the effect of different droplet sizes on the final equilibrium position, Y_e^*, of the droplet at $H_0 = 50\,000$ A/m and $\lambda = 1$ along different arbitrary directions. As we have seen before in Fig. 4(a), at $\lambda = 1$, in the absence of a magnetic field, the droplet settles at a position between the bottom wall and center of the channel, but Fig. 12 shows that as the droplet size increases, it moves closer to the center; however, when the size of the droplet is comparable enough to the width of the channel, i.e., $R_0^* = 0.24$, it migrates toward the centerline, which is also consistent with the findings in the literature [23]. Moreover, if we apply a constant magnetic field strength along different arbitrary directions in addition to varying sizes of the droplet, the results show that it is possible to efficiently separate droplets at different positions along the channel based on the deformation and orientation of the droplet.

4. Effect of viscosity ratio

The viscosity ratio plays an important role in the experimental analyses that deal with the behavior of drops of different fluids suspended in another fluid [14,22]. Here we investigate the contribution of viscosity ratios on the steady-state position of the droplet in a parabolic flow under the effect of a uniform magnetic field along different directions. In order to perform this analysis, the relative size of the droplet is kept constant, i.e., $R_0^* = 0.15$, while the magnetic field is applied along arbitrary directions for different viscosity ratios.

At first, we apply the magnetic field in a direction parallel to the flow field to observe its effect on the migration behavior

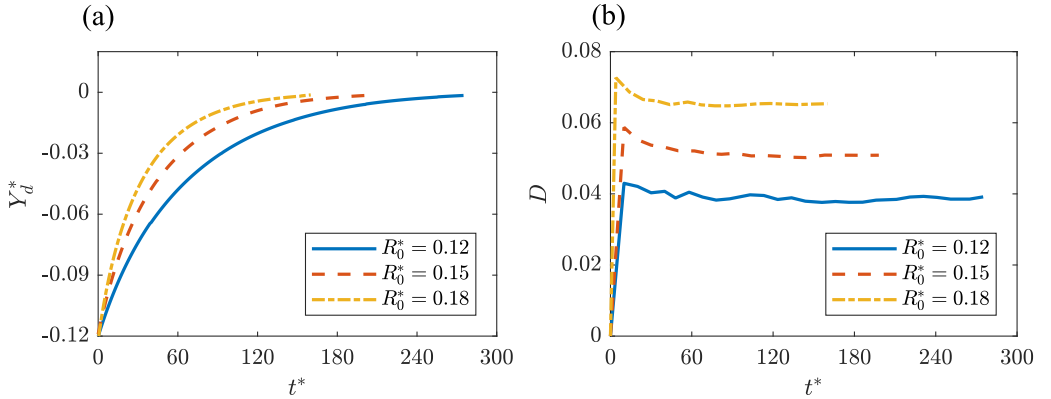

FIG. 11. Effect of droplet sizes, R_0^*, on the migration behavior of the droplet at $\alpha = 90^\circ$, $\mathrm{Re}_d = 0.03$, and $\lambda = 1$. (a) Y_d^* vs. t^* and (b) D vs. t^*.

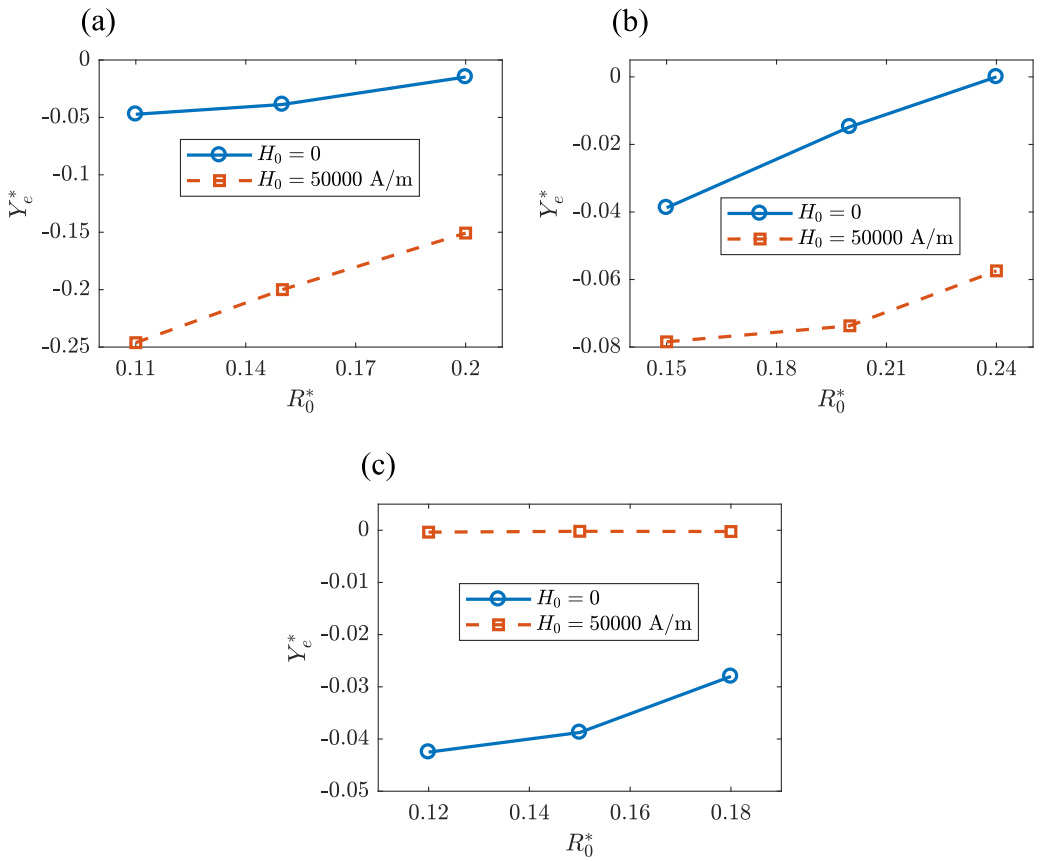

FIG. 12. Effect of droplet sizes, R_0^*, on the final equilibrium position, Y_e^*, of the droplet at $H_0 = 50000$ A/m and $\lambda = 1$. (a) $\alpha = 0^\circ$, (b) $\alpha = 45^\circ$, and (c) $\alpha = 90^\circ$.

of the droplet. Figure 13(a) illustrates the effect of different viscosity ratios on the lateral migration behavior of the droplet at $\alpha = 0^\circ$. From Fig. 13(a), it can be seen that at a fixed magnetic Bond number, Bo_m, as the viscosity ratio increases, the droplet starts to migrate away from the center of the channel, and at a higher magnetic Bond number, i.e., $\mathrm{Bo}_m > 8$, it settles closer to the wall. This is because when the magnetic field is applied at $\alpha = 0^\circ$, the steady-state deformation of the droplet increases with the increase of viscosity ratio at a fixed Bo_m, which in turn helps the droplet to settle closer to the wall. Interestingly, the equilibrium position starts to overlap with each other at a critical magnetic Bond number, i.e., $\mathrm{Bo}_{\mathrm{cr}} \approx 7$, and a reverse trend appears where the droplet with higher viscosity is found to settle further away from the bottom wall compared to the lower viscous drops. This happens because as the viscosity ratio increases, the increased droplet deformation at a higher magnetic Bond number reduces the clearance space between the droplet and the bottom wall. As a result, the force exerted by the wall increases, which ultimately pushes the droplet away from the wall toward the center of the flow domain.

Figure 13(b) represents the effect of different viscosity ratios on the lateral migration behavior of the droplet at $\alpha = 45^\circ$. Without a magnetic field (i.e., $\mathrm{Bo}_m = 0$), at $\lambda = 0.5$ and 1 the droplet settles at a position between the center and bottom wall of the channel, while at $\lambda = 0.05$, the final equilibrium position is located at the center. These results are also consistent with the findings of Chan and Leal [17]. Also, with the decrease in viscosity ratios, the droplet moves closer to the center of the channel. But in the presence of a magnetic field, the droplet presents an interesting migration behavior. Figure 13(b) shows that at $\lambda = 0.5$ and 1, as the magnetic Bond number Bo_m increases, the droplet starts to move away from the center, and at a certain magnetic Bond number, i.e., $\mathrm{Bo}_m \approx 8.72$, it changes its migration direction back toward the center of the channel. We found that there exists a critical steady-state deformation (i.e., $D_{\mathrm{cr}} \approx 0.12$) where this behavior appears. Additionally, as the magnetic field strength increases past that critical point, at a fixed magnetic Bond number Bo_m, the final equilibrium position of the droplet moves closer to the center of the channel as the viscosity ratio decreases. On the other hand, when $\lambda = 0.05$, the droplet starts to cross the center of the channel as soon as the magnetic field is applied, and as magnetic bond number increases, the droplet moves further away from the center. In this case, the asymmetry of the droplet shape helps the droplet cross the center of the channel.

Now we investigate the effect of different viscosity ratios on the final equilibrium position of the droplet with the magnetic field applied perpendicularly to the flow field direction (i.e., $\alpha = 90^\circ$). Figure 13(c) shows that in the presence of a magnetic field, the droplet finds an equilibrium position exactly at the center of the channel for all different viscosity ratios. This happens because as soon as the magnetic field is applied the droplet undergoes deformation and tries to orient itself along the direction of the magnetic field, thus

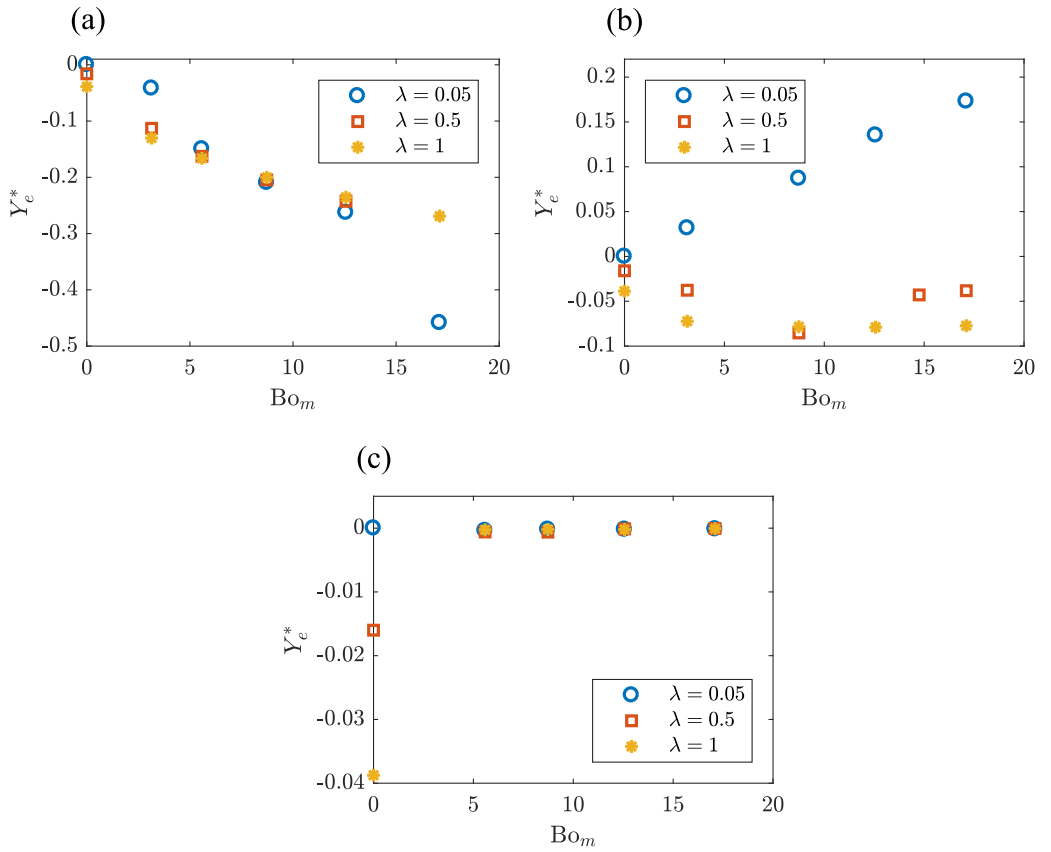

FIG. 13. Effect of viscosity ratios, λ, on the final equilibrium position, Y_e^*, of the droplet at $R_0^* = 0.15$ and $\mathrm{Re}_d = 0.03$. (a) $\alpha = 0^\circ$, (b) $\alpha = 45^\circ$, and (c) $\alpha = 90^\circ$.

resulting in a symmetric shape, which in turn aids the droplet in maintaining its position at the center. Furthermore, with decreasing viscosity ratio, the droplet reaches its final equilibrium position faster in the channel.

Last, an overview on the dependence of lateral migration behavior of a droplet in a channel flow on the deformation D and orientation angle θ is illustrated in Fig. 14. Figure 14(a) shows that in the absence of any external forces ($\mathrm{Re}_d = 0.03$, $\mathrm{Bo}_m = 0$), D and θ are dependent on the viscosity ratio λ and capillary number Ca [i.e., $(D, \theta) = f(\lambda, \mathrm{Ca})$], which ultimately contribute in determining the final equilibrium position of droplet in a Poiseuille flow. On the other hand, in the absence of any external flows ($\mathrm{Re}_d = 0$) in Fig. 14(b), the magnetic field defines the shape of a droplet, while the orientation angle is defined by the magnetic field direction [i.e., $(D, \theta) = f(\lambda, \mathrm{Bo}_m, \alpha)$]. As a result, in Fig. 14(c), under the combined effect of flow and magnetic fields, the lateral migration behavior of droplet becomes more complex where the final equilibrium position is dictated by the viscosity ratio λ, capillary number Ca, magnetic Bond number Bo_m, and magnetic field direction α (i.e., $Y_e^* = f(D, \theta) = f(\lambda, \mathrm{Ca}, \mathrm{Bo}_m, \alpha)$). Additionally, the final equilibrium positions of droplet under variable magnetic field strengths at $\mathrm{Re}_d = 0.03$ and $\lambda = 1$ are portrayed in Fig. 15, which further demonstrate the dependence of final equilibrium position on the shape and orientation of droplet in a channel.

V. CONCLUSION

The lateral migration of a ferrofluid droplet in a plane Poiseuille flow under the influence of a uniform magnetic field along several directions is systematically studied in this paper. In the absence of a magnetic field, the droplet finds its equilibrium position at a location between the center and bottom wall of the channel for $\lambda = 0.5$ and 1, while at $\lambda = 0.05$ it settles at the center of the channel. Applying a magnetic field along arbitrary directions results in different final equilibrium positions in the channel due to the different alignments of the droplet with the flow field. As we increase the magnetic field strength along $\alpha = 0^\circ$, at a viscosity ratio $\lambda = 1$, the final equilibrium position of the droplet moves closer to the bottom wall of the channel. However, if we apply the magnetic field along $\alpha = 45^\circ$, then the droplet moves closer to the center of the channel as the magnetic field strength is increased. Eventually, if the magnetic field is applied along $\alpha = 90^\circ$, then the droplet will find its equilibrium position exactly at the center of the flow domain. The droplet will reach the equilibrium position faster as the magnetic field strength increases due to the increased deformation at a higher magnetic Bond number. We also found that at a fixed viscosity ratio $\lambda = 1$, in the absence of any magnetic field, as the droplet size increases, the droplet moves closer to the center of channel, and if the

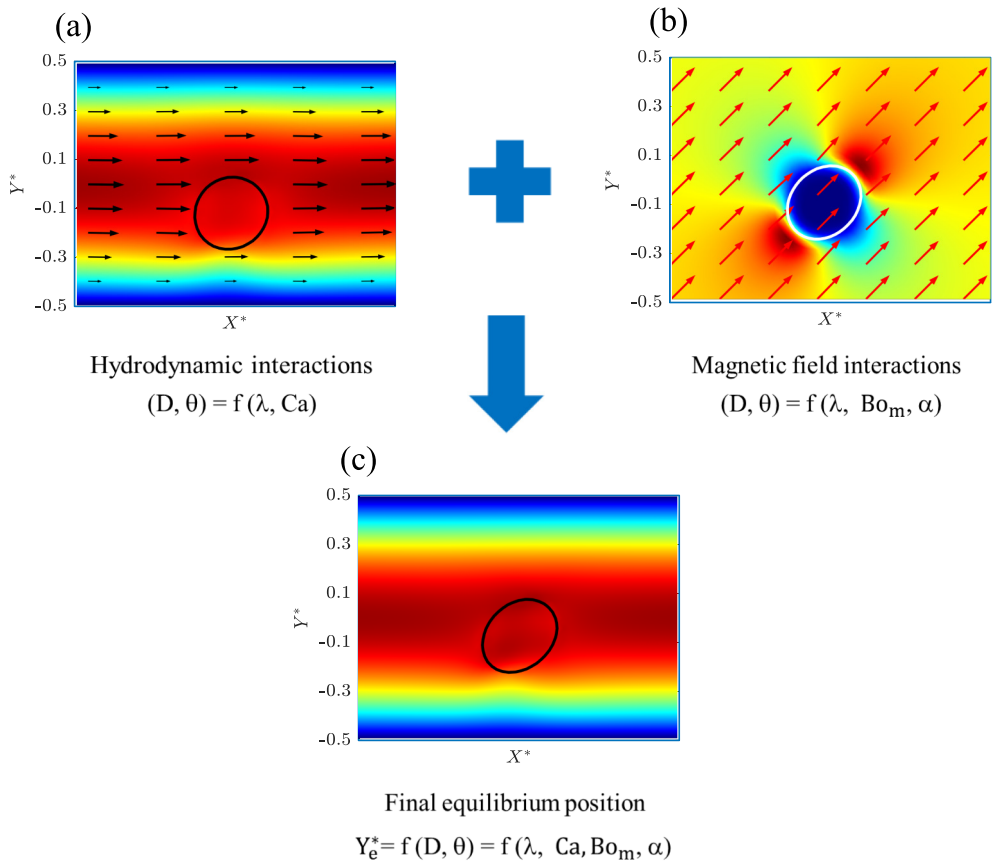

FIG. 14. Dependence of lateral migration behavior of a droplet on deformation D and orientation angle θ in a channel flow. (a) Pressure-driven flow, $\mathrm{Re}_d = 0.03$, $\mathrm{Bo}_m = 0$, $\lambda = 1$, where the arrow size is proportional to the velocity in the domain; (b) droplet under magnetic field, $\mathrm{Re}_d = 0$, $\mathrm{Bo}_m = 17.1$, $\alpha = 45^\circ$, $\lambda = 1$; and (c) final equilibrium position of droplet, $\mathrm{Re}_d = 0.03$, $\mathrm{Bo}_m = 17.1$, $\alpha = 45^\circ$, $\lambda = 1$.

droplet size becomes comparable enough to the width of the channel, i.e., $R_0^* = 0.24$, it settles at the center of the flow domain. Furthermore, if we apply a constant magnetic field strength along arbitrary directions with variable drop sizes, it helps manipulate the final equilibrium position of the droplet along the channel. For example, at $\alpha = 0^\circ$ a smaller sized droplet settles closer to the wall due to reduced steady-state deformation. On the other hand, at $\alpha = 45^\circ$, as the droplet size increases, the droplet moves closer to the center of the channel, while at $\alpha = 90^\circ$, the equilibrium position is found at the center for all drop sizes.

Furthermore, we investigated the effect of different viscosity ratios on the lateral migration behavior of the droplet under the influence of a uniform magnetic field at arbitrary directions and found that for a fixed droplet size at $\alpha = 0^\circ$, the droplet moves closer to the bottom wall with decreasing viscosity ratios. At $\alpha = 45^\circ$, we observed an interesting behavior for $\lambda = 0.5$ and 1 where the direction of migration changes at a critical steady-state deformation and migrates back toward the center. However, if the magnetic field is applied along 45° at $\lambda = 0.05$, then the droplet crosses the center and settles on the other side of the channel due to the asymmetry of the droplet shape. Finally, at $\alpha = 90^\circ$, the final equilibrium position of the droplet is found at the center of the channel irrespective of different viscosity ratios. The different lateral migration behavior results suggest an efficient but simple means of separating the ferrofluid droplets from nonmagnetic droplets along different lateral positions in the channel based on different magnetic field direction, magnetic field strength, droplet size, and viscosity ratio at microscale.

ACKNOWLEDGMENTS

The authors gratefully acknowledge the financial support from the Department of Mechanical and Aerospace Engineering (MAE) and the Center for Biomedical Research (CBR) at Missouri University of Science and Technology. This work is partially supported by the National Science Foundation (Grant No. DMS-1818642).

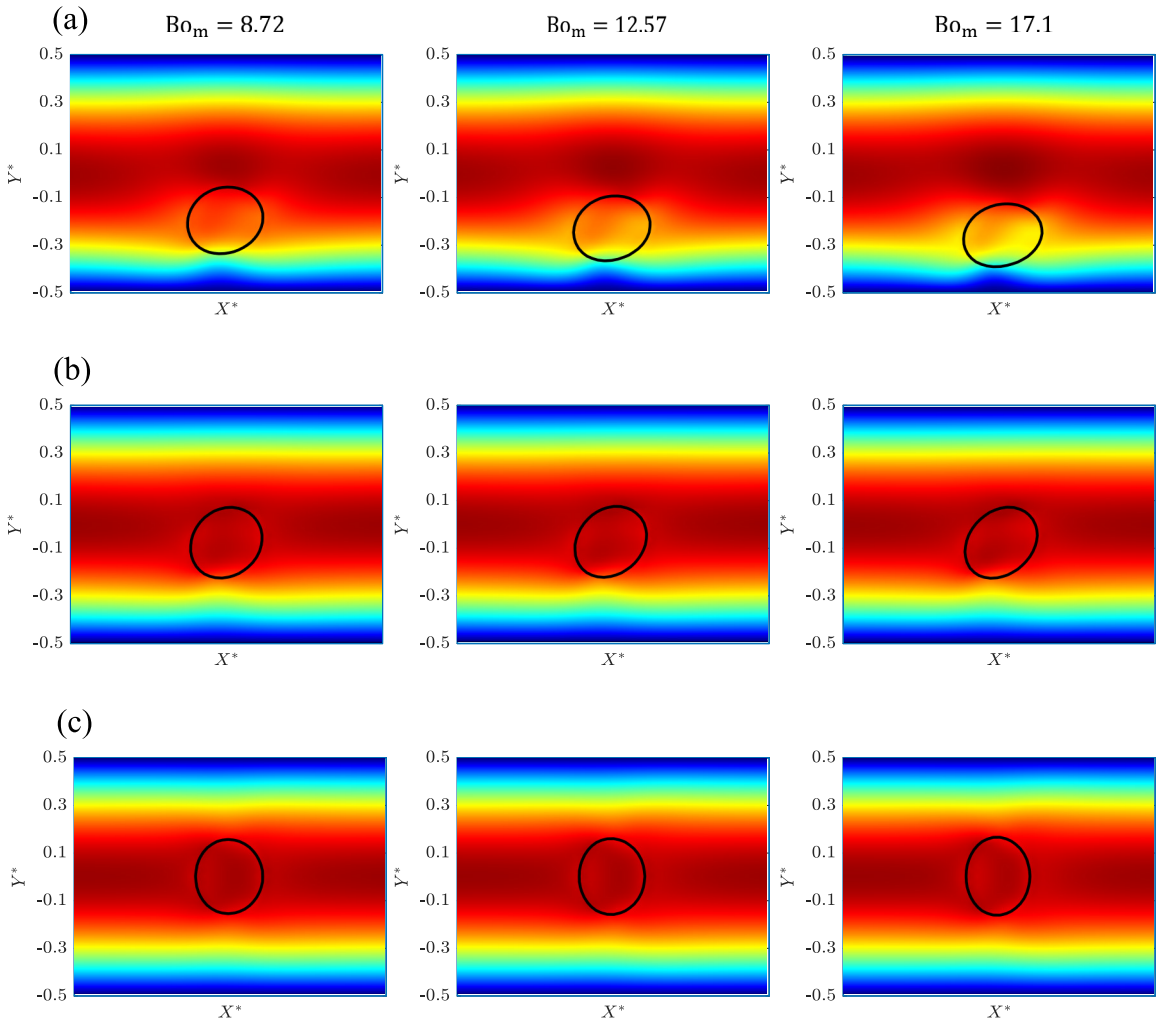

FIG. 15. Final equilibrium positions of droplet under variable magnetic bond numbers Bo_m at $Re_d = 0.03$ and $\lambda = 1$. (a) $\alpha = 0°$, (b) $\alpha = 45°$, and (c) $\alpha = 90°$.

[1] T. F. Tadros, Industrial applications of dispersions, Adv. Colloid Interface Sci. **46**, 1 (1993).

[2] O. Skurtys and J. Aguilera, Applications of microfluidic devices in food engineering, Food Biophys. **3**, 1 (2008).

[3] P. J. Hailing and P. Walstra, Protein-stabilized foams and emulsions, Crit. Rev. Food Sci. Nutr. **15**, 155 (1981).

[4] L. L. Schramm, *Emulsions, Foams, and Suspensions: Fundamentals and Applications* (John Wiley & Sons, 2006).

[5] A. Abeynaike, A. Sederman, Y. Khan, M. Johns, J. Davidson, and M. Mackley, The experimental measurement and modeling of sedimentation and creaming for glycerol/biodiesel droplet dispersions, Chem. Eng. Sci. **79**, 125 (2012).

[6] S. Less and R. Vilagines, The electrocoalescers' technology: Advances, strengths and limitations for crude oil separation, J. Pet. Sci. Eng. **81**, 57 (2012).

[7] P. Atten, Electrocoalescence of water droplets in an insulating liquid, J. Electrost. **30**, 259 (1993).

[8] K. Lissant, Emulsions and emulsion technology, Soil Sci. **120**, 160 (1975).

[9] R. Skalak, N. Ozkaya, and T. C. Skalak, Biofluid mechanics, Annu. Rev. Fluid Mech. **21**, 167 (1989).

[10] A. Karnis and S. Mason, Particle motions in sheared suspensions: Xxiii. Wall migration of fluid drops, J. Colloid Interface Sci. **24**, 164 (1967).

[11] C. Chaffey, H. Brenner, and S. Mason, Particle motions in sheared suspensions, Rheol. Acta **4**, 64 (1965).

[12] Y. Wang and P. Dimitrakopoulos, Low-reynolds-number droplet motion in a square microfluidic channel, Theor. Comput. Fluid Dyn. **26**, 361 (2012).

[13] S. D. Hudson, Wall migration and shear-induced diffusion of fluid droplets in emulsions, Phys. Fluids **15**, 1106 (2003).

[14] S. Guido and V. Preziosi, Droplet deformation under confined poiseuille flow, Adv. Colloid Interface Sci. **161**, 89 (2010).

[15] C. Coulliette and C. Pozrikidis, Motion of an array of drops through a cylindrical tube, J. Fluid Mech. **358**, 1 (1998).

[16] R. Khayat, A. Luciani, and L. Utracki, Boundary-element analysis of planar drop deformation in confined flow. Part 1. Newtonian fluids, Eng. Anal. Bound. Elem. **19**, 279 (1997).

[17] P.-H. Chan and L. Leal, The motion of a deformable drop in a second-order fluid, J. Fluid Mech. **92**, 131 (1979).
[18] O. S. Pak, J. Feng, and H. A. Stone, Viscous marangoni migration of a drop in a poiseuille flow at low surface péclet numbers, J. Fluid Mech. **753**, 535 (2014).
[19] J. A. Hanna and P. M. Vlahovska, Surfactant-induced migration of a spherical drop in stokes flow, Phys. Fluids **22**, 013102 (2010).
[20] H. Zhou and C. Pozrikidis, The flow of suspensions in channels: Single files of drops, Phys. Fluids A **5**, 311 (1993).
[21] H. Zhou and C. Pozrikidis, The flow of ordered and random suspensions of two-dimensional drops in a channel, J. Fluid Mech. **255**, 103 (1993).
[22] H. Zhou and C. Pozrikidis, Pressure-driven flow of suspensions of liquid drops, Phys. Fluids **6**, 80 (1994).
[23] S. Mortazavi and G. Tryggvason, A numerical study of the motion of drops in poiseuille flow. Part 1. Lateral migration of one drop, J. Fluid Mech. **411**, 325 (2000).
[24] S. Afkhami, A. Leshansky, and Y. Renardy, Numerical investigation of elongated drops in a microfluidic t-junction, Phys. Fluids **23**, 022002 (2011).
[25] M. Kennedy, C. Pozrikidis, and R. Skalak, Motion and deformation of liquid drops, and the rheology of dilute emulsions in simple shear flow, Comput. Fluids **23**, 251 (1994).
[26] H. Goldsmith and S. Mason, The flow of suspensions through tubes. i. single spheres, rods, and discs, J. Colloid Sci. **17**, 448 (1962).
[27] W. Hiller and T. Kowalewski, An experimental study of the lateral migration of a droplet in a creeping flow, Exp. Fluids **5**, 43 (1986).
[28] W. Olbricht, Pore-scale prototypes of multiphase flow in porous media, Annu. Rev. Fluid Mech. **28**, 187 (1996).
[29] M. R. Hassan and C. Wang, Magnetic field induced ferrofluid droplet breakup in a simple shear flow at a low reynolds number, Phys. Fluids **31**, 127104 (2019).
[30] M. R. Hassan and C. Wang, Ferro-hydrodynamic interactions between ferrofluid droplet pairs in simple shear flows, Colloids Surf. A **602**, 124906 (2020).
[31] H. A. Stone, J. R. Lister, and M. P. Brenner, Drops with conical ends in electric and magnetic fields, Proc. R. Soc. Lond. A **455**, 329 (1999).
[32] P. M. Vlahovska, On the rheology of a dilute emulsion in a uniform electric field, J. Fluid Mech. **670**, 481 (2011).
[33] S. Mandal, A. Bandopadhyay, and S. Chakraborty, The effect of uniform electric field on the cross-stream migration of a drop in plane poiseuille flow, J. Fluid Mech. **809**, 726 (2016).
[34] J. Q. Feng, Electrohydrodynamic behavior of a drop subjected to a steady uniform electric field at finite electric reynolds number, Proc. R. Soc. Lond. A **455**, 2245 (1999).
[35] J.-C. Bacri, D. Salin, and R. Massart, Study of the deformation of ferrofluid droplets in a magnetic field, J. Phys. Lett. **43**, 179 (1982).
[36] S. Afkhami, A. Tyler, Y. Renardy, M. Renardy, T. S. Pierre, R. Woodward, and J. Riffle, Deformation of a hydrophobic ferrofluid droplet suspended in a viscous medium under uniform magnetic fields, J. Fluid Mech. **663**, 358 (2010).
[37] A. Zakinyan and Y. Dikansky, Drops deformation and magnetic permeability of a ferrofluid emulsion, Colloids Surf. A **380**, 314 (2011).
[38] O. T. Mefford, R. C. Woodward, J. D. Goff, T. Vadala, T. G. S. Pierre, J. P. Dailey, and J. S. Riffle, Field-induced motion of ferrofluids through immiscible viscous media: Testbed for restorative treatment of retinal detachment, J. Magn. Magn. Mater. **311**, 347 (2007).
[39] J. Liu, Y. F. Yap, and N.-T. Nguyen, Numerical study of the formation process of ferrofluid droplets, Phys. Fluids **23**, 072008 (2011).
[40] S. Afkhami, Y. Renardy, M. Renardy, J. Riffle, and T. St Pierre, Field-induced motion of ferrofluid droplets through immiscible viscous media, J. Fluid Mech. **610**, 363 (2008).
[41] D. Shi, Q. Bi, and R. Zhou, Numerical simulation of a falling ferrofluid droplet in a uniform magnetic field by the voset method, Numer. Heat Transf. A **66**, 144 (2014).
[42] M. R. Hassan, J. Zhang, and C. Wang, Deformation of a ferrofluid droplet in simple shear flows under uniform magnetic fields, Phys. Fluids **30**, 092002 (2018).
[43] J. Zhang, M. R. Hassan, B. Rallabandi, and C. Wang, Migration of ferrofluid droplets in shear flow under a uniform magnetic field, Soft Matter **15**, 2439 (2019).
[44] S. Van der Graaf, T. Nisisako, C. Schroen, R. Van Der Sman, and R. Boom, Lattice boltzmann simulations of droplet formation in a t-shaped microchannel, Langmuir **22**, 4144 (2006).
[45] R. Van der Sman and S. Van der Graaf, Emulsion droplet deformation and breakup with lattice boltzmann model, Comput. Phys. Commun. **178**, 492 (2008).
[46] COMSOL, CFD Module Application Library Manual, 5th ed.
[47] R. E. Rosensweig, *Ferrohydrodynamics* (Cambridge University Press, Cambridge, 1985).
[48] J. A. Stratton, *Electromagnetic Theory* (John Wiley & Sons, New York, 2007).
[49] G. I. Taylor, The viscosity of a fluid containing small drops of another fluid, Proc. R. Soc. Lond. Ser. A **138**, 41 (1932).
[50] G. I. Taylor, The formation of emulsions in definable fields of flow, Proc. R. Soc. Lond. Ser. A **146**, 501 (1934).